# Influence of the dissipative topological edge state on quantized transport in $MnBi_2Te_4$

Weiyan Lin,[1,*] Yang Feng,[2,8,*] Yongchao Wang,[4,*] Zichen Lian,[3] Hao Li,[5,6] Yang Wu,[6,7] Chang Liu,[3,8] Yihua Wang,[2,9] Jinsong Zhang,[3,10] Yayu Wang,[3,10] Xiaodong Zhou,[1,12,13,†] and Jian Shen[1,2,9,11,12,13,‡]

[1]*State Key Laboratory of Surface Physics and Institute for Nanoelectronic Devices and Quantum Computing, Fudan University, Shanghai, China*

[2]*Department of Physics, Fudan University, Shanghai, China*

[3]*State Key Laboratory of Low Dimensional Quantum Physics, Department of Physics, Tsinghua University, Beijing, China*

[4]*Beijing Innovation Center for Future Chips, Tsinghua University, Beijing, China*

[5]*School of Materials Science and Engineering, Tsinghua University, Beijing, China*

[6]*Tsinghua-Foxconn Nanotechnology Research Center, Department of Physics, Tsinghua University, Beijing, China*

[7]*Department of Mechanical Engineering, Tsinghua University, Beijing, China*

[8]*Beijing Academy of Quantum Information Science, Beijing, China*

[9]*Shanghai Research Center for Quantum Sciences, Shanghai, China*

[10]*Frontier Science Center for Quantum Information, Beijing, China*

[11]*Collaborative Innovation Center of Advanced Microstructures, Nanjing, China*

[12]*Shanghai Qi Zhi Institute, Shanghai, China*

[13]*Zhangjiang Fudan International Innovation Center, Fudan University, Shanghai, China*

(Received 13 January 2022; accepted 28 March 2022; published 11 April 2022)

The beauty of the quantum Hall (QH) effect is the metrological precision of Hall resistance quantization that originates from the topological edge states. Understanding the factors that lead to quantization breakdown not only provides important insights on the nature of the topological protection of these edge states, but is beneficial for device applications involving such quantized transport. In this work, we combine conventional transport and real space conductivity mapping to investigate whether the quantization breakdown is tied to the disappearance of edge state in the hotly studied $MnBi_2Te_4$ system. Our experimental results unambiguously show that topological edge state does exist when quantization breakdown occurs. Such edge state is dissipative in nature and could lead to a quantization breakdown due to its diffusive character causing overlapping with bulk and other edge states in real devices. Our findings bring attention to issues that are generally inaccessible in the transport study of QH, but can play important roles in practical measurements and device applications.

DOI: 10.1103/PhysRevB.105.165411

## I. INTRODUCTION

Similar to the quantum Hall (QH) effect [1], the quantum anomalous Hall (QAH) effect [2,3] originates from the topologically protected chiral edge state. The QAH phase was firstly established in magnetically doped topological insulator (TI), although its onset temperature remains significantly lower than the Curie temperature despite tremendous efforts to raise it [4–7]. While such quantization breakdown, i.e., deviation from $h/e^2$ in $R_{yx}$, is generally attributed to the dissipation added to the chiral edge conduction [8], much remains unknown regarding the source of such dissipations. Early nonlocal transport has suggested the existence of a dissipative nonchiral edge mode [9,10]. However, this edge-dominated dissipation picture was later challenged by transport using Corbino geometry which identified bulk conduction as the dominant source of dissipation [11]. Another source of dissipation comes from the magnetic disorder leading to strong spatial fluctuations of exchange energy gap [12,13]. An essential question is whether the chiral edge state could survive with such disorders. This issue becomes relevant for intrinsic magnetic TI $MnBi_2Te_4$ [14–17], where angle-resolved photoemission spectroscopy fails to detect the exchange gap in its surface Dirac cone below Néel temperature [18–20], casting doubts on its supremacy in terms of the magnetic ordering. Moreover, a multidomain state could form inside the material resulting in a complex network of conducting edge channel that would affect the quantized transport as well [21,22].

In this work, we investigate the underlying mechanism of quantization breakdown in $MnBi_2Te_4$ which can be viewed as layered TI $Bi_2Te_3$ with each of its Te-Bi-Te-Bi-Te quintuple layers intersected by a Mn-Te bilayer, forming Te-Bi-Te-Mn-Te-Bi-Te septuple layer (SL). The magnetic moment of Mn orders ferromagnetically (FM) within each SL, and antiferromagnetically (AFM) between neighboring SL. When all the Mn moments are aligned parallel by an external magnetic field, $MnBi_2Te_4$ is driven to a Chern insulator with quantized Hall resistance. The zero-field QAH has been observed on 5-SL $MnBi_2Te_4$ at 1.4 K [23]. Under external field, this

*These authors contributed equally to this work.
†zhouxd@fudan.edu.cn
‡shenj5494@fudan.edu.cn

 ©2022 American Physical Society

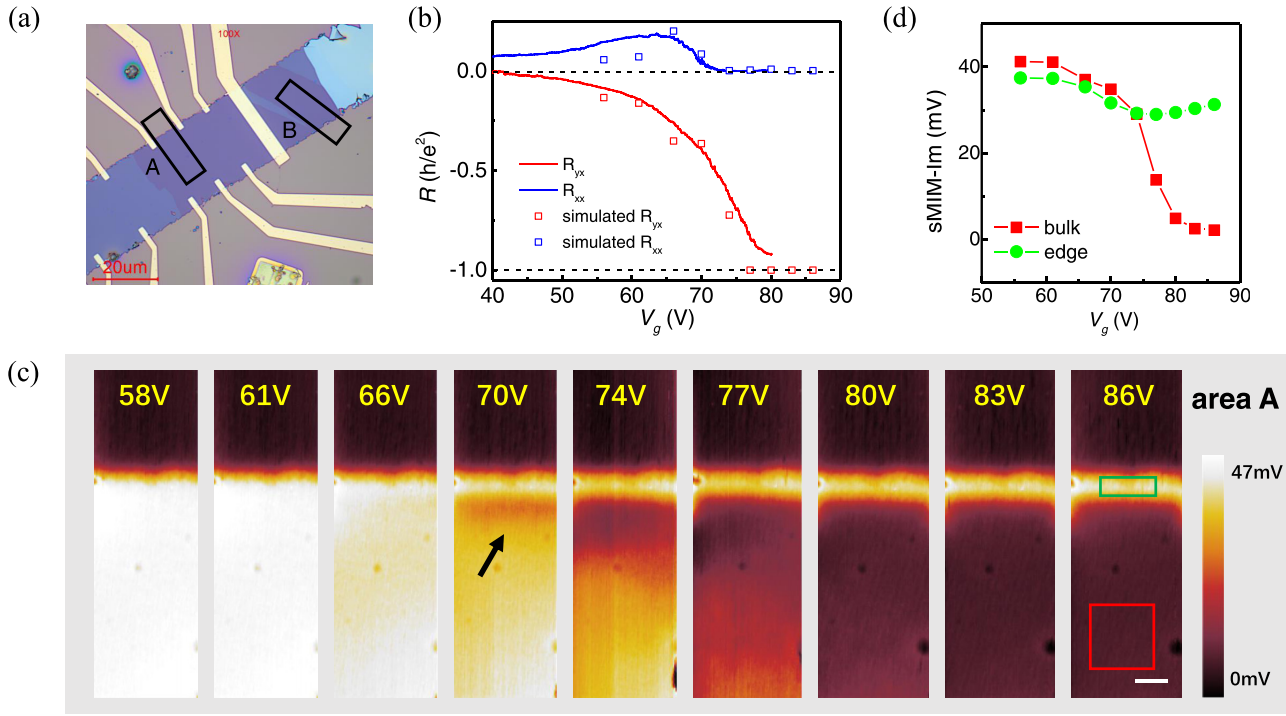


FIG. 1. (a) Optical image of sample I. (b) Gate-voltage dependent longitudinal resistance $R_{xx}$ and Hall resistance $R_{yx}$ at 1.7 K, 9 T, and the Landauer-Buttiker model simulation results. (c) Gate-voltage dependent sMIM images at 1.7 K, 9 T of area A marked in (a). Area with the electric field focusing is denoted by the black arrow. Scale bar is 2 $\mu$m. (d) Gate-voltage dependent sMIM bulk (edge) signal averaged from the red (green) rectangular area denoted in (c).

quantization temperature can go up to a few tens of kelvin, an encouraging sign for potential applications [24,25]. The AFM ground state of $MnBi_2Te_4$ is also a topological phase different from the Chern insulator. Previous transport measurement has identified a zero-Hall plateau (ZHP) on 6-SL $MnBi_2Te_4$ in its AFM state, suggesting an axion insulator [26]. More interestingly, a dissipative edge state was recently reported in such a ZHP phase by nonlocal transport [27] and scanning microwave impedance microscopy (sMIM) studies [28]. Different from previous works, we complement conventional transport with real space conductivity mapping to acquire local conducting properties essential for interpreting global transport behavior. By observing how the quantized transport is "destroyed" by gating and elevating temperature, we identify the dissipative edge state as the origin of the observed quantization breakdown, rather than the multidomain state or the absence of the edge conduction channel. We also discuss the influence of such dissipative channel on the edge conduction in real devices giving insights to the observed transport behavior.

## II. RESULTS AND DISCUSSION

We first look at the gate-voltage dependent transport and sMIM characterization of the Chern insulator phase. sMIM is a recently developed scanning probe microscopy combining atomic force microscopy and scanning near-field optical microscopy working in the microwave (∼GHz) range [29]. A 3-GHz microwave signal is delivered to the tip apex and interacts with the sample area underneath the tip. Its reflected signal is collected and demodulated into imaginary and real channels (sMIM-Im and sMIM-Re). Such signal measures the screening property of a local small area which is intimately related to its local conductivity. Therefore, sMIM can be employed to perform local conductivity mapping with nanoscale spatial resolution and is powerful to distinguish an insulating bulk from a conducting edge in topological systems [30]. In this work, sMIM-Im is chosen as the signal as it increases monotonically with increasing conductivity. Figure 1(a) is an optical image of one $MnBi_2Te_4$ sample (sample I), on which the transport and sMIM data were measured from the 6-SL thickness area (purple color). Figure 1(b) shows the gate-voltage dependent longitudinal resistance $R_{xx}$ and Hall resistance $R_{yx}$ measured at 1.7 K and 9 T. As expected, $R_{yx}$ gradually approaches the quantized value $h/e^2$ with increasing gate voltage while $R_{xx}$ vanishes at the same time. What is unusual is that $R_{xx}$ seems to be quantized after $V_g = +74V$ while $R_{yx}$ continues to rise from $V_g = +74$ V to $V_g = +80$ V. This behavior is in contradiction to conventional wisdom that quantization of $R_{xx}$ and $R_{yx}$ should happen simultaneously. We have checked this behavior by looking at $R_{xx}$ and $R_{yx}$ measured from other electrodes on the device and reached the same conclusion (see Supplemental Material [31]). This helps us to rule out carrier inhomogeneity as the origin of such a quantization shift [32]. To understand such transport behavior, we use sMIM to probe the gate evolution of conducting properties at microscopic scale. Figure 1(c) shows a series of gate-dependent sMIM images taken at 1.7 K and 9 T in the area A marked in Fig. 1(a). Here, larger sMIM signal corresponds to higher local conductivity. The sample's interior (bulk) changes from a metallic to an insulating state as its chemical potential moves into the gap by gating. At the

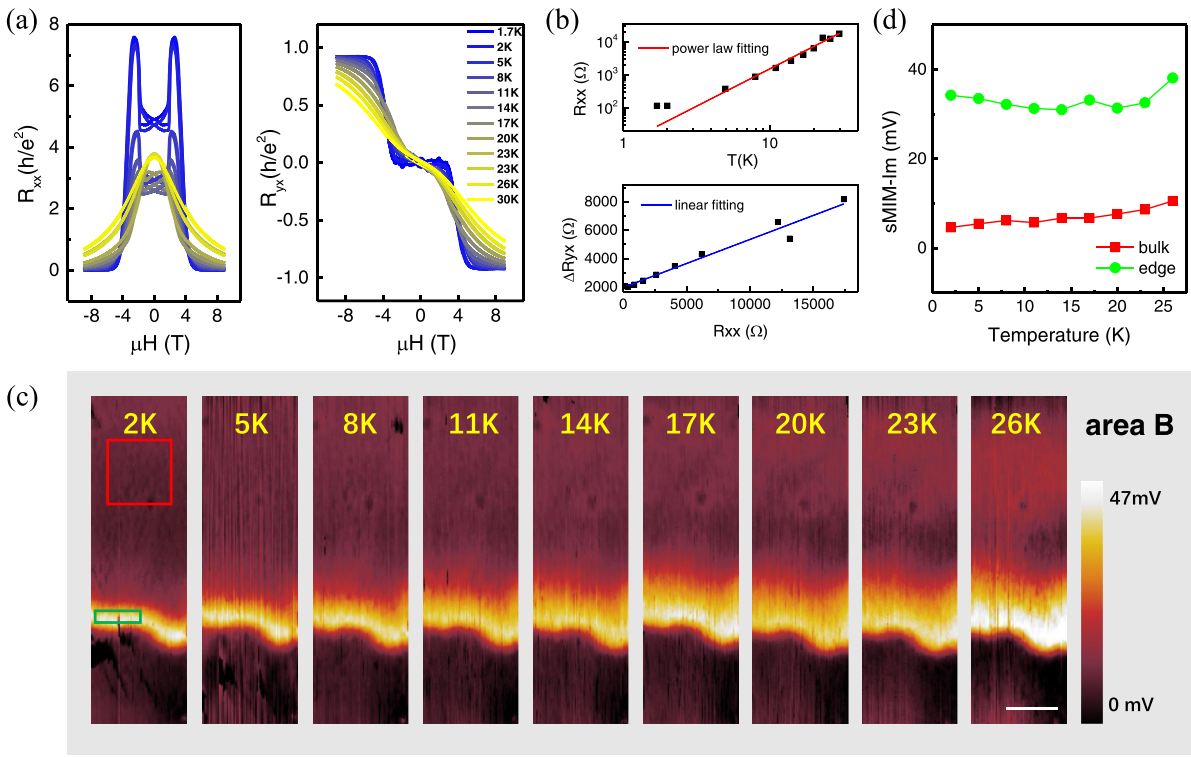


FIG. 2. (a) Longitudinal $R_{xx}$ and Hall resistance $R_{yx}$ vs magnetic field acquired at various temperatures taken at +80-V gate voltage. (b) Power-law fitting of $R_{xx}(T)$ at 9 T and the linear relationship between $R_{xx}$ and $\Delta R_{yx}$ in the Chern insulator phase. (c) Temperature-dependent sMIM images at +80-V gate voltage, 9-T of area B marked in Fig. 1(a). Scale bar is 4 $\mu$m. (d) Temperature-dependent sMIM bulk (edge) signal averaged from the red (green) rectangular area denoted in (c).

same time, a persistent metallic state exists at the sample's edge corresponding to the in-gap topological edge state. What is more, the sample edge experiences a stronger electric field and thus a larger effective doping. As shown in Fig. 1(c), the insulating area of the bulk first appears near the edges and then spreads inwards. An intriguing situation happens at $V_g = +70$ V where a conductive bulk and a metallic edge are spatially separated by an insulating strip in between. This situation becomes more apparent at $V_g = +74$ V. This inhomogeneous gating originates from a geometric effect [33] and is of particular relevance for our transport measurement as discussed below. In Fig. 1(d), we extract the bulk and edge sMIM signals and plot them as a function of the gate voltage. These sMIM signals can be converted to real conductivity (see Supplemental Material [31]). In a gating experiment, the Hall quantization breakdown, i.e., deviation from $h/e^2$ in $R_{yx}$, is usually attributed to the bulk conduction. If one compares $R_{yx}$ in Fig. 1(b) to sMIM-bulk in Fig. 1(d), they indeed show a very similar gate-voltage dependence indicating their close relationship. We examine this relationship by performing a model simulation to calculate $R_{yx}$ and $R_{xx}$ using the measured bulk and edge conductivity (see Supplemental Material [31]). This model adopts Landauer-Buttiker formalism to describe the ballistic transport of chiral edge channels. The conducting bulk is treated as a parallel channel with the edge modifying the transmission probability between two terminals as done before [8]. In Fig. 1(b), the simulated results lay nicely over the transport curves except for $R_{yx}$ at higher gate voltages. In particular, this model reproduces the $V_g = +74$ V case where $R_{xx}$ is quantized to 0 while $R_{yx}$ is only 0.75 $h/e^2$. This can be understood in the following picture. At $V_g = +74$ V, the device possesses two spatially separated current flow channels. Roughly 75% of injected current goes along the dissipationless edge while the remaining 25% goes through the bulk. Since there is no crosstalk between the edge and bulk channel, the edge channel remains dissipationless and thus already "quantized," giving vanishingly small $R_{xx}$ and contributing to 0.75 $h/e^2$ in $R_{yx}$. As the bulk becomes more insulating at higher gate voltages, more current will flow along the edge and the quantized value of $R_{yx}$ will increases accordingly. Our model predicts a 100% quantization of $R_{yx}$ after $V_g = +77$ V based on the measured bulk conductivity while the experiment does not reach this level, indicating residual bulk current [34,35]. Nevertheless, our sMIM imaging and model simulation corroborate the belief that the bulk conduction is a major source of Hall quantization breakdown in a gating experiment. More importantly, it highlights the importance of knowing the actual current flow in real devices to understand the seemingly counterintuitive transport results.

We next investigate the temperature dependence of the Chern insulator phase, which is mostly relevant to quantization breakdown. The fact that QAH temperature of $MnBi_2Te_4$ is still much lower than its Curie temperature falls short of the expectation for this stoichiometric compound and leaves open various possibilities to account for such discrepancy. Here we use sMIM imaging to narrow down the possible scenarios. Figure 2(a) shows $R_{xx}$ and $R_{yx}$ versus temperature

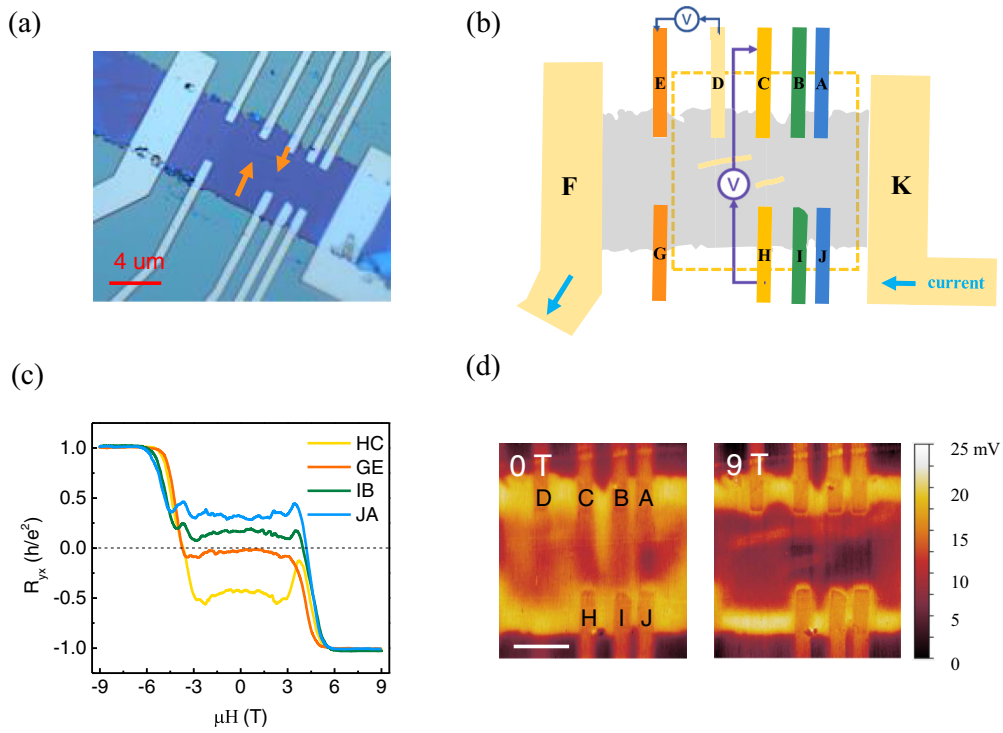


FIG. 3. (a) Optical image of sample II. Orange arrows indicate cracks inside the device. (b) Schematic of transport measurement setup. sMIM scan field of view is marked by dashed orange square. (c) Hall resistance $R_{yx}$ as a function of magnetic field for four pairs of electrodes taken at 1.7 K and +25-V gate voltage. (d) sMIM images of crack area taken at 1.7 K, 0 T, +14-V gate voltage and 1.7 K, 9 T, +20-V gate voltage, respectively. Scale bar is 4 $\mu$m.

and magnetic field on the same device shown in Fig. 1. At 1.7 K, this 6-SL $MnBi_2Te_4$ displays a magnetic field-driven topological phase transition from a ZHP phase with $C = 0$ to a Chern insulator phase with $C = 1$. A clear plateau-to-plateau transition happens in $R_{yx}(H)$. When the temperature increases, this plateau-to-plateau transition becomes broad, signaling the quantization breakdown. Following previous attempts of QH analysis [36], we plot $R_{xx}(9T)$ as a function of temperature in a log-log scale in the upper panel of Fig. 2(b). The data points fall naturally on a straight line, indicating a power-law dependence on temperature. Previous temperature-dependent QH study has seen a change from a power law to an exponential dependence of $R_{xx}(T)$ as the temperature increases [36], corresponding to a crossover from variable-range hopping to thermal activation behavior of charge transport. The fact that we only see a power law up to 30 K implies that thermal activation is still "frozen out" in this temperature range. In the bottom panel of Fig. 2(b), we plot $\Delta R_{yx}$, which is the deviation of $R_{yx}$ from $h/e^2$, and $R_{xx}$ together. A linear relationship has been observed similar to QH systems before [37,38]. This empirical result reconfirms the consensus that quantization breakdown in QH system is due to the dissipation. What remains to be answered is the source of such dissipation.

Our sMIM imaging provides clue to origins of dissipation. Figure 2(c) shows the sMIM images of the Chern insulator phase at various temperatures. They look almost identical with an insulating bulk interior surrounded by a conductive edge. The only change perceived from these images is the widening edge state with increasing temperatures. Such apparent width in sMIM images cannot be taken as a real physical dimension of topological edge state, but rather a measure of how metallic edge states penetrate into the insulating bulk. We apply a Gaussian fit to extract such penetration depth of edge states which increases from 2 to 3 $\mu$m in this temperature range (see Supplemental Material [31]). In regarding the dissipation source, the sMIM observation has the following implications. First, this quantization breakdown is not caused by the absence of chiral edge state which continues to exist even if $R_{yx}$ is far below $h/e^2$ at high temperatures. Similar conclusion has been drawn in magnetically doped TI system [39]. Second, there is no internal current flow due to the formation of multidomain states. Our magnetic field-dependent sMIM images further rule out such multidomain state in our device (see Supplemental Material [31]). Actually, for magnetic materials in the ultrathin limit, magnetic anisotropy will dominate over dipolar interaction to form a single-domain state [40]. Third, bulk conduction should be insignificant. Figure 2(d) shows the extracted bulk and edge sMIM signals versus temperature. Considering that sMIM signal is proportional to the log scale of sample's conductivity (see Supplemental Material [31]), this plot indicates that the bulk conductivity is four orders of magnitude smaller than the edge conductivity in the whole temperature range. Last but not least, we can only identify a widening edge state as an experimental signature which strongly suggests an edge-related dissipation mechanism leading to a diffusive edge channel. For instance, a recent theoretical work considers the thermal spin fluctuations as the origin of quantization breakdown at high temperatures [41]. Such thermal spin fluctuations act as frozen magnetic disorders that scatter the chiral edge state and facilitate its

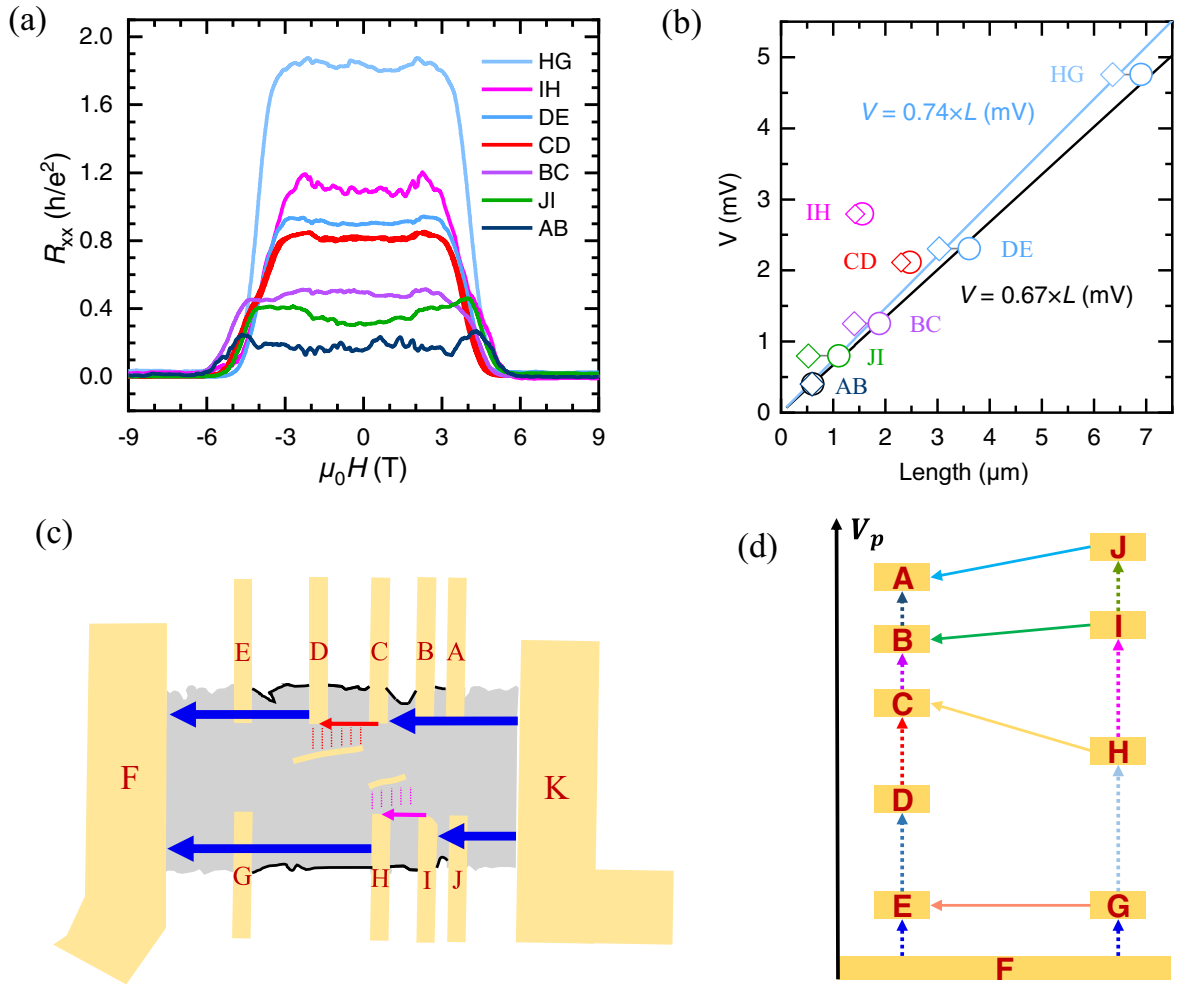


FIG. 4. (a) Longitudinal resistance $R_{xx}$ as a function of magnetic field for seven pairs of electrodes taken at 1.7 K and +25-V gate voltage. (b) Voltage drop at zero field of various pairs of electrodes as a function of the distance between two electrodes in a pair (diamonds) or the length of sample boundary connecting neighboring electrodes (circles). A linear fitting to the data is a manifestation of Ohm's law. (c) Schematic of current flow pattern in the device at zero field. Red shadow and pink shadow represent the interaction between sample boundaries and internal cracks. Solid black lines denote the contour of the sample boundary between neighboring electrodes. (d) Schematic of relative potential among various electrodes.

overlapping with the bulk states, which may be the origin of quantization breakdown.

The gating and temperature-dependent experiments above illustrate the need of preserving a dissipationless nature of edge state in achieving a quantized transport in $MnBi_2Te_4$. We now show another experiment to make this point clearer. Figure 3(a) is the optical image of another 6-SL $MnBi_2Te_4$ (sample II) with multiple pairs of electrodes for transport characterizations. Different from sample I, two cracks exist in the interior of this device, denoted by orange arrows in Fig. 3(a). We note that sample II has been studied in our previous work in which we reported a conducting edge state at zero field challenging the axion insulator assignment to ZHP phase [28]. We argue that, instead of axion insulator, even-layer $MnBi_2Te_4$ at zero field is in an AFM quantum spin Hall (QSH) state hosting a pair of helical edge states with strong dissipations. In this work, we report additional transport results concerning the quantized transport in such a device. Figure 3(b) is a schematic of the transport setup with all the electrodes properly marked. We run the current from source $K$ to drain $F$ and measure Hall resistance $R_{yx}$ from a pair of opposite-placed electrodes perpendicular to the current flow. In Fig. 3(c), we plot $R_{yx}(H)$ measured from four pairs of electrodes (GE, HC, IB, and JA). While the overall shapes of $R_{yx}(H)$ are similar with a clear plateau-to-plateau transition, there exists a systematic voltage offset for ZHP among those electrodes. For electrodes that are further from the cracks such as GE, we obtain the correct $R_{yx}(H)$ as reported before [26]. Such $R_{yx}(H)$ of GE was also reported in our previous work [28]. For electrodes that sit near the cracks (HC, IB, and JA), however, there is an offset for ZHP. Interestingly, such offset only happens for ZHP, but not for the Chern insulator phase, i.e., $R_{yx}(H)$ from four pairs of electrodes all collapse to $h/e^2$ plateau at high fields. We note that $R_{yx}(H)$ in Fig. 3(c) are raw data without antisymmetrization as routinely applied in Hall measurement. Such antisymmetrization in $R_{yx}$ is intended to remove components symmetric with magnetic field, i.e., $R_{xx}$ components. For example, the misalignment of opposite-placed Hall electrodes along current flow direction usually gives rise to such artifacts which should be removed

by antisymmetrization. However, the systematic ZHP offset we observe here cannot be attributed to this problem as seen in the optical image. Instead, it reflects the property pertaining to this device which we will discuss as below. We also rule out magnetic hysteresis as the origin of the ZHP offset as reported in a previous work [42]. We show the $R_{yx}(H)$ of HC, GE, IB, and JA at both positive and negative scanning-field directions in the supplement (see Supplemental Material [31]). Those curves do not have any magnetic hysteresis. Furthermore, we adopt a scanning superconducting quantum interference device (sSQUID) to directly measure the static magnetic flux generated by net magnetization of the sample (see Supplemental Material [31]). Being an ultrasensitive probe of magnetization, sSQUID provides an important check to our even- or odd-layer thickness determination of $MnBi_2Te_4$ devices. Indeed, sample II has negligible magnetization consistent with its even-layer property in which no magnetic hysteresis is expected. Figure 3(d) shows sMIM images acquired from the crack area, which are taken at 0 and 9 T corresponding to ZHP and Chern insulator phase, respectively. Note that such sMIM images have been reported in our previous work showing edge states in both ZHP and Chern insulator phases [28]. The most important feature revealed in such imaging is that the dissipative edge state of ZHP phase is spatially more extended than the dissipationless chiral edge state of Chern insulator phase. In addition, we see a conductive strip along the crack in both ZHP and Chern insulator phase corresponding to the topological edge state. This difference in terms of the dissipation level of edge states has a dramatic consequence on the charge transport in the device.

For a better understanding, let us start with $R_{xx}$ shown in Fig. 4(a) as a function of magnetic field for seven pairs of electrodes. They all vanish at high fields, signaling a dissipationless edge state in the Chern insulator phase. However, $R_{xx}$ acquires a finite value at ZHP phase due to the dissipative nature of the edge channel. For a dissipative edge, we expect $R_{xx}$ to follow Ohm's law, i.e., its resistance value (or voltage drop $V$ for a given excitation current) is linearly proportional to the length $L$ of the edge. We first define such length as the longitudinal distance between the neighboring parallel electrodes shown as diamond points in Fig. 4(b). Only three of seven data points (AB, DE, and HG) seem to fall onto a straight line with the formula $V = 0.74 \times L$ following Ohm's law (its intercept must be 0), while the rest are away from the line. In light of the fact that a topological edge state (also current flowing path) will strictly follow the contour of the sample boundary, we improve the plot by redefining the length as the length of sample boundary connecting neighboring electrodes [solid black lines in Fig. 4(c)]. Such correction will shift the diamond points to the right [circles in Fig. 4(b)] due to the curved shape of the boundary. Now five of seven circle points (AB, JI, BC, DE, and HG) converge onto another straight line with the formula $V = 0.67 \times L$ following Ohm's law as well. The remaining two points, IH and CD, are still off the line displaying a larger resistance than expected, which leads us to consider extra dissipation source. We argue that the interaction between the crack and the sample boundary in these areas gives rise to the extra resistance. The diffusive character of edge state at zero field facilitates the overlapping between the crack and the sample boundary, ultimately causing a larger dissipation. In Fig. 4(d), we plot the relative voltage drop among those electrodes according to our analysis above which naturally explains the voltage offset for ZHP in Fig. 3(c). Our previous work suggests an AFM QSH origin of the edge state at zero field in 6-SL $MnBi_2Te_4$ [28]. Such helical edge state is less immune to the impurity scatterings which makes the quantized transport fragile [43]. On the other hand, for Chern insulator phase, the chirality of edge state makes it robust against backscattering and preserves its dissipationless nature explaining the nice quantization of $R_{xx}$ and $R_{yx}$ among those electrodes. As a comparison, sample I does not have a geometric defect (cracks) in device area and $R_{xx}$ measured between the electrodes fits Ohm's law nicely (see Supplemental Material [31]).

## III. CONCLUSION

We discuss the factors that may lead to quantization breakdown of topological edge conduction in $MnBi_2Te_4$. While the topological edge state can survive under different circumstances in the absence of quantization, preserving its dissipationless nature is the key to achieve quantized transport. One consequence of such dissipative edge state on quantized transport is to cause spatial overlapping between edge and the bulk state, resulting in unexpected transport behavior. Moreover, this work demonstrates sMIM as an important probe to complement the conventional transport. Knowing the microscopic details of the local current distribution is essential to comprehensively understand the behavior of global charge transport.

## ACKNOWLEDGMENTS

We acknowledge the discussions with C. Z. Chen and Y. H. Li. The work at Fudan University is supported by National Natural Science Foundation of China (Grants No. 12074080, No. 11804052, No. 11904053, and No. G11827805), National Postdoctoral Program for Innovative Talents (Grant No. BX20180079), Shanghai Science and Technology Committee Rising-Star Program (Grant No. 19QA1401000), Major Project (Grant No. 2019SHZDZX01), and Ministry of Science and Technology of China (Grants No. 2016YFA0301002 and No. 2017YFA0303000). The work at Tsinghua University is supported by National Natural Science Foundation of China (Grants No. 21975140 and No. 51991343), the Basic Science Center Project of National Natural Science Foundation of China (Grant No. 51788104), and the National Key R&D Program of China (Grant No. 2018YFA0307100).

[1] K. von Klitzing, G. Dorda, and M. Pepper, Phys. Rev. Lett. **45**, 494 (1980).

[2] C. X. Liu, X. L. Qi, X. Dai, Z. Fang, and S. C. Zhang, Phys. Rev. Lett. **101**, 146802 (2008).

[3] R. Yu, W. Zhang, H. J. Zhang, S. C. Zhang, X. Dai, and Z. Fang, Science **329**, 61 (2010).

[4] C. Z. Chang, J. S. Zhang, X. Feng, J. Shen, Z. C. Zhang, M. H. Guo, K. Li, Y. B. Ou, P. Wei, L. L. Wang, Z. Q. Ji, Y. Feng, S. H. Ji, X. Chen, J. F. Jia, X. Dai, Z. Fang, S. C. Zhang, K. He, Y. Y. Wang, L. Lu, X. C. Ma, and Q. K. Xue, Science **340**, 167 (2013).

[5] J. G. Checkelsky, R. Yoshimi, A. Tsukazaki, K. S. Takahashi, Y. Kozuka, J. Falson, M. Kawasaki, and Y. Tokura, Nat. Phys. **10**, 731 (2014).

[6] X. F. Kou, S. T. Guo, Y. B. Fan, L. Pan, M. R. Lang, Y. Jiang, Q. M. Shao, T. X. Nie, K. Murata, J. S. Tang, Y. Wang, L. He, T. K. Lee, W. L. Lee, and K. L. Wang, Phys. Rev. Lett. **113**, 137201 (2014).

[7] C. Z. Chang, W. W. Zhao, D. Y. Kim, H. J. Zhang, B. A. Assaf, D. Heiman, S. C. Zhang, C. X. Liu, M. H. W. Chan, and J. S. Moodera, Nat. Mater. **14**, 473 (2015).

[8] J. Wang, B. Lian, H. J. Zhang, and S. C. Zhang, Phys. Rev. Lett. **111**, 086803 (2013).

[9] C. Z. Chang, W. W. Zhao, D. Y. Kim, P. Wei, J. K. Jain, C. X. Liu, M. H. W. Chan, and J. S. Moodera, Phys. Rev. Lett. **115**, 057206 (2015).

[10] S. W. Wang, D. Xiao, Z. W. Dou, M. D. Cao, Y. F. Zhao, N. Samarth, C. Z. Chang, M. R. Connolly, and C. G. Smith, Phys. Rev. Lett. **125**, 126801 (2020).

[11] L. K. Rodenbach, I. T. Rosen, E. J. Fox, P. Zhang, L. Pan, K. L. Wang, M. A. Kastner, and D. Goldhaber-Gordon, APL Mater. **9**, 081116 (2021).

[12] E. O. Lachman, A. F. Young, A. Richardella, J. Cuppens, H. R. Naren, Y. Anahory, A. Y. Meltzer, A. Kandala, S. Kempinger, Y. Myasoedov, M. E. Huber, N. Samarth, and E. Zeldov, Sci. Adv. **1**, e1500740 (2015).

[13] I. Lee, C. K. Kim, J. Lee, S. J. L. Billinge, R. D. Zhong, J. A. Schneeloch, T. S. Liu, T. Valla, J. M. Tranquada, G. D. Gu, and J. C. S. Davis, Proc. Natl. Acad. Sci. USA **112**, 1316 (2015).

[14] M. M. Otrokov, I. I. Klimovskikh, H. Bentmann, D. Estyunin, A. Zeugner, Z. S. Aliev, S. Gass, A. U. B. Wolter, A. V. Koroleva, A. M. Shikin, M. Blanco-Rey, M. Hoffmann, I. P. Rusinov, A. Y. Vyazovskaya, S. V. Eremeev, Y. M. Koroteev, V. M. Kuznetsov, F. Freyse, J. Sanchez-Barriga, I. R. Amiraslanov, M. B. Babanly, N. T. Mamedov, N. A. Abdullayev, V. N. Zverev, A. Alfonsov, V. Kataev, B. Buchner, E. F. Schwier, S. Kumar, A. Kimura, L. Petaccia, G. Di Santo, R. C. Vidal, S. Schatz, K. Kissner, M. Unzelmann, C. H. Min, S. Moser, T. R. F. Peixoto, F. Reinert, A. Ernst, P. M. Echenique, A. Isaeva, and E. V. Chulkov, Nature (London) **576**, 416 (2019).

[15] Y. Gong, J. W. Guo, J. H. Li, K. J. Zhu, M. H. Liao, X. Z. Liu, Q. H. Zhang, L. Gu, L. Tang, X. Feng, D. Zhang, W. Li, C. L. Song, L. L. Wang, P. Yu, X. Chen, Y. Y. Wang, H. Yao, W. H. Duan, Y. Xu, S. C. Zhang, X. C. Ma, Q. K. Xue, and K. He, Chin. Phys. Lett. **36**, 076801 (2019).

[16] J. H. Li, Y. Li, S. Q. Du, Z. Wang, B. L. Gu, S. C. Zhang, K. He, W. H. Duan, and Y. Xu, Sci. Adv. **5**, eaaw5685 (2019).

[17] D. Q. Zhang, M. J. Shi, T. S. Zhu, D. Y. Xing, H. J. Zhang, and J. Wang, Phys. Rev. Lett. **122**, 206401 (2019).

[18] Y. J. Hao, P. F. Liu, Y. Feng, X. M. Ma, E. F. Schwier, M. Arita, S. Kumar, C. W. Hu, R. E. Lu, M. Zeng, Y. Wang, Z. Y. Hao, H. Y. Sun, K. Zhang, J. W. Mei, N. Ni, L. S. Wu, K. Shimada, C. Y. Chen, Q. H. Liu, and C. Liu, Phys. Rev. X **9**, 041038 (2019).

[19] H. Li, S.-Y. Gao, S.-F. Duan, Y.-F. Xu, K.-J. Zhu, S.-J. Tian, J.-C. Gao, W.-H. Fan, Z.-C. Rao, J.-R. Huang, J.-J. Li, D.-Y. Yan, Z.-T. Liu, W.-L. Liu, Y.-B. Huang, Y.-L. Li, Y. Liu, G.-B. Zhang, P. Zhang, T. Kondo, S. Shin, H.-C. Lei, Y.-G. Shi, W.-T. Zhang, H.-M. Weng, T. Qian, and H. Ding, Phys. Rev. X **9**, 041039 (2019).

[20] Y. J. Chen, L. X. Xu, J. H. Li, Y. W. Li, H. Y. Wang, C. F. Zhang, H. Li, Y. Wu, A. J. Liang, C. Chen, S. W. Jung, C. Cacho, Y. H. Mao, S. Liu, M. X. Wang, Y. F. Guo, Y. Xu, Z. K. Liu, L. X. Yang, and Y. L. Chen, Phys. Rev. X **9**, 041040 (2019).

[21] X. F. Kou, L. Pan, J. Wang, Y. B. Fan, E. S. Choi, W. L. Lee, T. X. Nie, K. Murata, Q. M. Shao, S. C. Zhang, and K. L. Wang, Nat. Commun. **6**, 8474 (2015).

[22] J. Wang, B. Lian, and S. C. Zhang, Phys. Rev. B **89**, 085106 (2014).

[23] Y. J. Deng, Y. J. Yu, M. Z. Shi, Z. X. Guo, Z. H. Xu, J. Wang, X. H. Chen, and Y. B. Zhang, Science **367**, 895 (2020).

[24] J. Ge, Y. Z. Liu, J. H. Li, H. Li, T. C. Luo, Y. Wu, Y. Xu, and J. Wang, Natl. Sci. Rev. **7**, 1280 (2020).

[25] Z. Ying, S. Zhang, B. Chen, B. Jia, F. Fei, M. Zhang, H. Zhang, X. Wang, and F. Song, Phys. Rev. B **105**, 085412(2022).

[26] C. Liu, Y. C. Wang, H. Li, Y. Wu, Y. X. Li, J. H. Li, K. He, Y. Xu, J. S. Zhang, and Y. Y. Wang, Nat. Mater. **19**, 522 (2020).

[27] Y. Li, C. Liu, Y. Wang, Z. Lian, H. Li, Y. Wu, J. Zhang, and Y. Wang, arXiv:2105.10390.

[28] W. Lin, Y. Feng, Y. Wang, Z. Lian, H. Li, Y. Wu, C. Liu, Y. Wang, J. Zhang, Y. Wang, X. Zhou, and J. Shen, arXiv:2105.10234 (2021).

[29] K. Lai, W. Kundhikanjana, H. Peng, Y. Cui, M. A. Kelly, and Z. X. Shen, Rev. Sci. Instrum. **80**, 043707 (2009).

[30] M. E. Barber, E. Y. Ma, and Z. X. Shen, Nat. Rev. Phys. **4**, 61 (2021).

[31] See Supplemental Material at http://link.aps.org/supplemental/10.1103/PhysRevB.105.165411 for additional transport, sMIM, and sSQUID experimental data, model calculation of longitudinal and Hall resistance, and Gaussian fit of edge state width.

[32] L. Galletti, T. Schumann, D. A. Kealhofer, M. Goyal, and S. Stemmer, Phys. Rev. B **99**, 201401(R) (2019).

[33] I. J. Vera-Marun, P. J. Zomer, A. Veligura, M. H. D. Guimaraes, L. Visser, N. Tombros, H. J. van Elferen, U. Zeitler, and B. J. van Wees, Appl. Phys. Lett. **102**, 013106 (2013).

[34] I. T. Rosen, M. P. Andersen, L. K. Rodenbach, L. Tai, P. Zhang, K. L. Wang, M. A. Kastner, and D. Goldhaber-Gordon, arXiv:2112.13123.

[35] G. M. Ferguson, R. Xiao, A. R. Richardella, D. Low, N. Samarth, and K. C. Nowack, arXiv:2112.13122.

[36] J. Matthews and M. E. Cage, J. Res. Natl. Inst. Stand. Technol. **110**, 497 (2005).

[37] V. M. Pudalov, S. G. Semenchinsky, A. N. Kopchikov, M. A. Vernikov, and L. M. Pazinich, Sov. Phys. JETP **62**, 630 (1985).

[38] M. E. Cage, B. F. Field, R. F. Dziuba, S. M. Girvin, A. C. Gossard, and D. C. Tsui, Phys. Rev. B **30**, 2286 (1984).

[39] K. M. Fijalkowski, N. Liu, P. Mandal, S. Schreyeck, K. Brunner, C. Gould, and L. W. Molenkamp, Nat. Commun. **12**, 5599 (2021).

[40] Q. Li, M. M. Yang, C. Gong, R. V. Chopdekar, A. T. N'Diaye, J. Turner, G. Chen, A. Schol, P. Shafer, E. Arenholz, A. K. Schmid, S. Wang, K. Liu, N. Gao, A. S. Admasu, S. W. Cheong, C. Y. Hwang, J. Li, F. Wang, X. Zhang, and Z. Q. Qiu, Nano Lett. **18**, 5974 (2018).

[41] Y.-H. Li and R. Cheng, Phys. Rev. Lett. **126**, 026601 (2021).

[42] A. Y. Gao, Y. F. Liu, C. W. Hu, J. X. Qiu, C. Tzschaschel, B. Ghosh, S. C. Ho, D. Berube, R. Chen, H. P. Sun, Z. W. Zhang, X. Y. Zhang, Y. X. Wang, N. Z. Wang, Z. M. Huang, C. Felser, A. Agarwal, T. Ding, H. J. Tien, A. Akey, J. Gardener, B. Singh, K. Watanabe, T. Taniguchi, K. S. Burch, D. C. Bell, B. B. Zhou, W. B. Gao, H. Z. Lu, A. Bansil, H. Lin, T. R. Chang, L. Fu, Q. Ma, N. Ni, and S. Y. Xu, Nature (London) **595**, 521 (2021).

[43] M. Konig, S. Wiedmann, C. Brune, A. Roth, H. Buhmann, L. W. Molenkamp, X. L. Qi, and S. C. Zhang, Science **318**, 766 (2007).